EAM-based multi-channel wavelength converter at 120 Gbps

VISHAL SHARMA[1], SURINDER SINGH[1,*], TARANJEET KAUR[2], VIKAS KUMAR GARG[3]
[1]*Department of ECE, Sant Longowal Institute of Engineering and Technology Longowal, Sangrur, Punjab, India*
[2]*Chandigarh Engineering College, Jhanjeri, India*
[3]*Department of CSE, Sant Longowal Institute of Engineering and Technology Longowal, Sangrur, Punjab, India*

A multi-channel wavelength conversion system operating at frequencies of 192.8 THz and 192.34 THz with a data rate of 120 Gbps is proposed using an electro-absorption modulator (EAM). The system achieves high-quality wavelength conversion with quality factors of 20.25 dB and 21.30 dB, respectively. A mathematical framework is developed to determine the sinusoidal signal generator frequency and maximum data signal bandwidth, ensuring minimal interference between wavelength-converted signals. The study demonstrates the potential of EAM for efficient, low-power, polarization-independent wavelength conversion in optical communication systems.

(Received October 10, 2025; accepted April 8, 2026)

Keywords: EAM modulator, XAM, Wavelength converter, All-optical signal processing

1. Introduction

High-speed all-optical signal processing operations are crucial for synchronous processing in high-speed optical networks [1-3]. Wavelength conversion is an essential technique to avoid contention in high-speed MIMO networks [1-3]. Various wavelength conversion techniques have been widely investigated, utilizing Kerr nonlinearities in semiconductor optical amplifiers (SOAs) and highly nonlinear fibers (HNLFs) for single-channel operations [4-14].

To date, researchers have proposed numerous wavelength conversion techniques exploiting cross-phase modulation (XPM) [9-13], cross-gain modulation (XGM) [14-16], and other Kerr nonlinearities [17, 18] in SOAs and HNLFs. All-optical wavelength converters based on four-wave mixing (FWM) have been explored in [4-8], emphasizing the need for phase-matching conditions to enhance FWM interactions between multiple signals within SOAs or HNLFs. However, achieving satisfactory wavelength conversion using FWM requires high pump and probe signal power, which adds to design complexity. In contrast, XPM-based wavelength converters, as proposed by various researchers [9-13], do not require phase-matching conditions, making them less complex compared to FWM. These converters typically employ Mach-Zehnder interferometric (MZI) configurations to achieve wavelength conversion. However, XPM interactions are highly sensitive to temperature and polarization states, resulting in output uncertainties and reduced reliability. To address challenges such as polarization dependency, complexity, and multichannel wavelength conversion, researchers have shifted towards electro-absorption modulator (EAM)-based wavelength converters. Seo et al. [18] investigated the efficiency of SOA-EAM-based wavelength conversion. Dahdah et al. [19] demonstrated all-optical wavelength conversion from 1310 nm to the C-band using XAM in an EAM. EAM-based converters offer numerous advantages over SOAs or optical fibers, including polarization independence, low power penalty, and high conversion efficiency. Lacey et al. [20] demonstrated polarization-independent multichannel wavelength conversion by exploiting FWM in SOAs. However, crosstalk and high power penalties remain significant challenges during multichannel wavelength conversion in SOAs and HNLFs [20]. Chow et al. [21] proposed wavelength conversion from a single wavelength to multiple wavelengths at a data rate of 10 Gbps. From the literature, it is evident that most prior work has focused on single-channel wavelength conversion using Kerr nonlinearities in SOAs or HNLFs. These polarization-dependent devices face significant challenges in performing multichannel wavelength conversion. In contrast, EAM-based wavelength conversion presents a promising alternative due to its polarization independence, high conversion efficiency, and low power penalty.

In the proposed design, we present an all-optical multichannel wavelength converter operating at a data rate of 120 Gbps by exploiting XAM within an EAM. While this work investigates wavelength conversion for AM modulation, future designs should support additional modulation formats.

2. EAM based multi-channel wavelength converter design

The basic block diagram for the multi-channel wavelength converter based on EAM is shown in Fig. 1. It consists of three sections: transmitter section, wavelength conversion section, and receiver section.

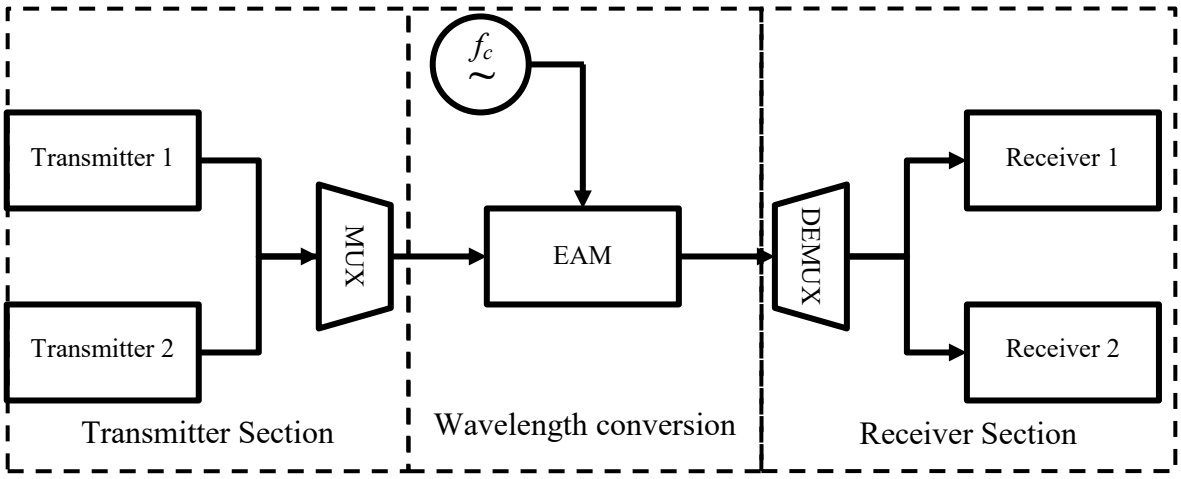

Fig. 1. Multi-channel wavelength converter block diagram

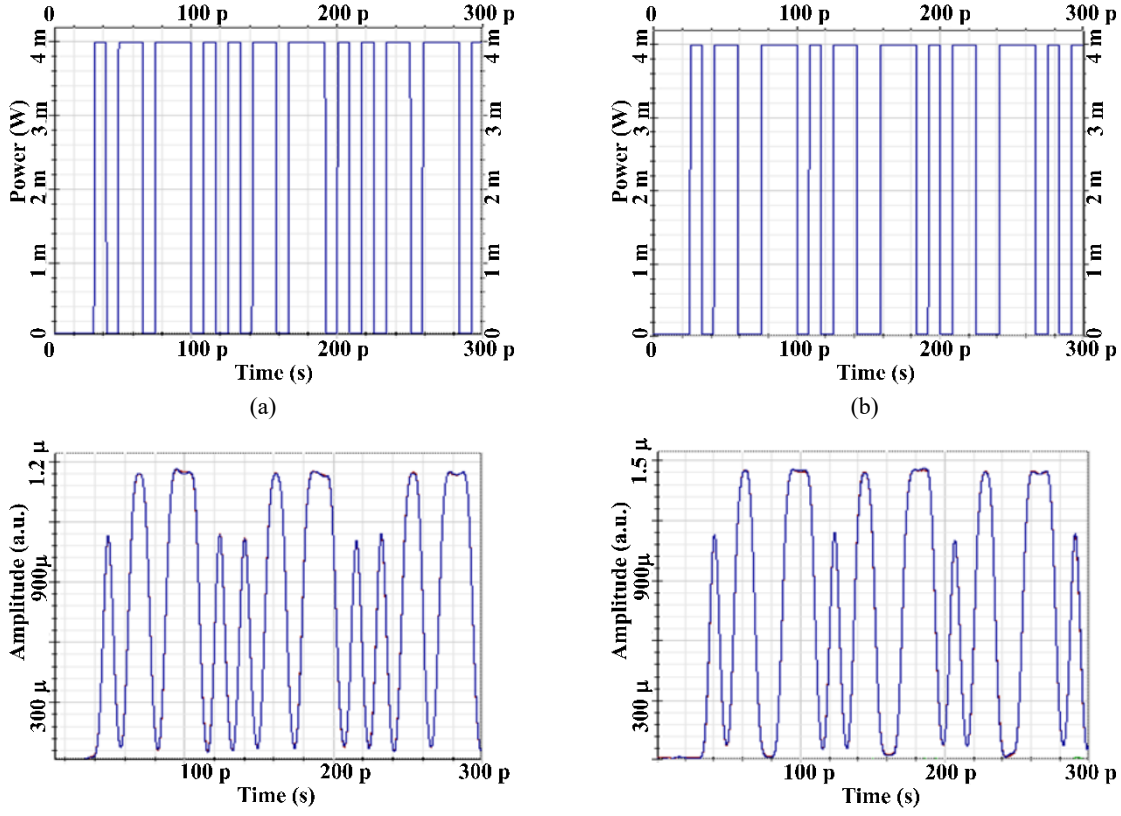

Fig. 2. Timing diagrams of signals at (a) Transmitter 1 (192.8 THz), (b) Transmitter 2 (192.34 THz), (c) Wavelength-converted signal at receiver 1 and (d) Wavelength-converted signal at receiver 2

The transmitter section consists of two transmitter blocks and a 2×1 multiplexer. Transmitter blocks define the signal sequence, transmission bit rate, signal modulation format, and system's operating frequency. In the proposed design, the transmitter section generates 120 Gbps NRZ formatted optical signals at centre frequencies of 192.8 THz and 193.34 THz. The input signal timing diagram is shown in Fig. 2 (a) and (b). The output signals from the transmission section are then passed to the wavelength conversion section. In this section, the multiplexed output signal propagates through the EAM modulator, which is controlled by a high-frequency sinusoidal electrical signal generator operating at 375 GHz. The frequency of the electrical signal generator must be chosen carefully to minimize or eliminate signal interference between the input and wavelength-converted signals. The appropriate frequency can be determined

using equations (1) to (6), which are derived based on interference conditions.

Let us consider f1 and f2 be the centre frequencis of two input message signals, where. There are two cases to analyze

Case I : **Widely spaced channels**

In this case system performance has been investigated for variable reverse bias voltage of EAM at fixed input power signal. The preset input power signal is 15 dBm and the reverse bias voltage is fixed commencing from 0.0 to 3.0 V is considered first for wavelength converted signal and the corresponding converted signal quality is shown in Fig. 3. Here the performance of converted wavelength at 1547 nm, 1548 nm, 1549 nm and 1550 nm is considered and reject the rest of converted wavelength due to degraded quality.

Channels are considered widely spaced if they follow the condition given in Equation (1).

$$f_2 - f_1 \geq \frac{3}{2}(B_1 + B_2) \tag{1}$$

$$f_c = \tfrac{3}{4}(f_2 - f_1) \tag{2}$$

$$B_{\max} = \frac{(f_2 - f_1)}{3} \tag{3}$$

Case II: Closely spaced channels

Channels are considered to be closely spaced when follow the condition given in equation (4).

$$f_2 - f_1 < \frac{3}{2}(B_1 + B_2) \tag{4}$$

$$f_c = \tfrac{3}{2}(f_2 - f_1) \tag{5}$$

$$B_{\max} = (f_2 - f_1) \tag{6}$$

Here in equation (1-6), f_c is the frequency of the electrical signal, B_1 and B_2 are the input signal optical bandwidth and B_{max} is the maximum bandwidth of the message signals.

The sinusoidal electrical signal controls the signal propagating through the EAM modulator. The EAM modulator employs a PIN structure, where the intrinsic region consists of an InGaAsP material-based quantum well structure designed for a wavelength range around 1550 nm [28]. Optical signal absorption occurs inside this intrinsic region. The PIN structure allows the application of a constant and high electric field (in the range of several kV/cm) across the intrinsic region [28, 29]. When a reverse-biased voltage is applied to the EAM modulator, a symmetrical tilt occurs in the conduction and valence bands of the quantum well, tilting toward the positive terminal of the modulator. This tilt increases the probability of carrier transitions due to the photon-assisted tunneling effect, even at low-frequency signals. This effect results in blue shifts in the excitonic absorption peaks of the EAM modulator's absorption spectrum, as shown in Fig. 3 [28, 29].

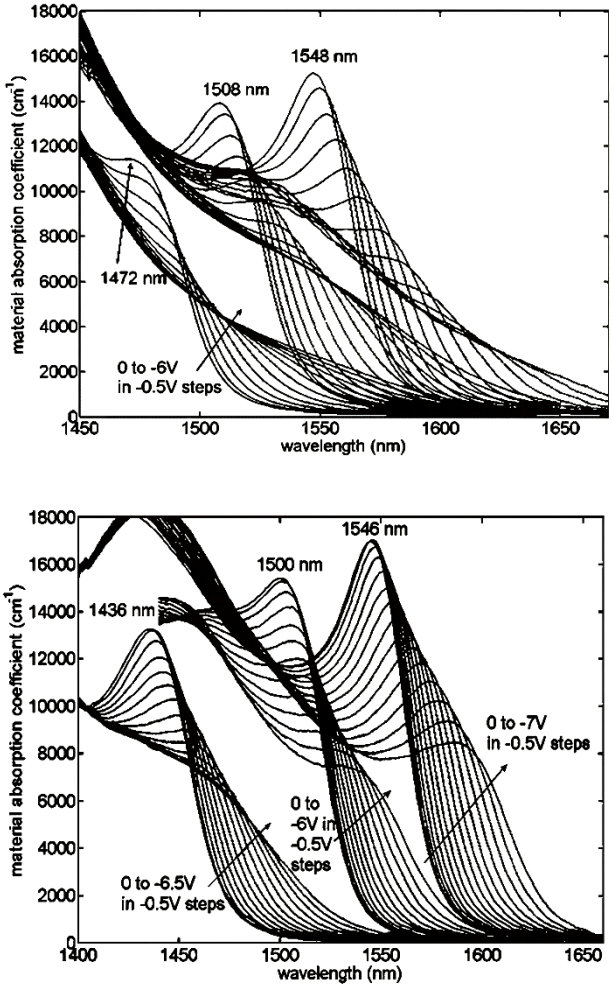

Fig. 3. Absorption spectrums of an EAM modulator at the quantum well structure of (a) 65 Å and (b) 90 Å [28].

From the Fig. 3, it can be observed that, with the increase in reverse biased voltage the blue shift also increases. The wavelength of an optical signal should lie somewhere in between the excitonic peak for 0 V and V_{max} (maximum reverse biased voltage). The V_{max} requirement increases with the increase in signal bit rate. The V_{max} should set in such a way that, the optical signal lies in between the excitonic peaks for 0 V and V_{max}.

The absorption of the optical signal strictly depends on the carrier rate equation of EAM. The number of photo generated carrier rate equation in the quantum well of EAM modulator depends on the absorption of the input signal which is given by equation (7) [30].

$$\frac{dN}{dt} = \frac{\lambda}{hc} 10^{-\frac{\Gamma_c}{10}} (1 - 10^{-(\Gamma(V,N) - 2\Gamma_c)}) P_{in} - \frac{N}{\tau} \tag{7}$$

Here in equation (7), N is the carrier concentration, $\frac{\lambda}{hc}$ is the energy of photon, Γ_c is the coupling loss, Γ is the voltage and carrier dependent fiber-to-fiber loss, and τ is the carrier escape time. Further, the electric field intensity $E(V)$ at the output port of EAM modulator can be calculated by equation (8) [30, 31].

$$E(V) = I(V)^{(1+j\alpha_m)/2} \tag{8}$$

Here, $I(V)$ is the voltage dependent intensity of optical signal which can be calculated by equation (9) and α_m is the alpha-parameter of EAM modulator which can be calculated by equation (10) [31].

$$I(V) = e^{(-\gamma(V)L)} \tag{9}$$

$$\alpha = \frac{\Delta n_r}{\Delta n_i} \tag{10}$$

Here, $\gamma(V)$ is the attenuation experienced by signal in EAM active medium, L is the product of the length of EAM modulator and its confinement factor, Δn_r is the change in the real part of refractive index and Δn_i is the change in the imaginary part of the refractive index of absorption layer due to the applied electric voltage. The output signal electric field intensity in terms of α_m and applied electric bias voltage can be calculated by equation (11) [31].

$$E(V) = \sqrt{I(V)}e^{(j\frac{1}{2}\int \alpha_m(V)d\log_e(I(V)))} \tag{11}$$

The equation (11) is the exact equation to calculate the output electric filed intensity but not suitable for simulation purpose. This equation requires the function evaluation and integration. The equation (11) can be modified as equation (12) [31, 32].

$$E(V) = I(V)^{(1+j\alpha_r(V))/2} \tag{12}$$

Here in equation (12), α_r is a function of α_m and voltage dependant attenuation constant $\gamma(V)$. The α_r can be calculated by equation (13) [31, 32].

$$\alpha_r(V) = \frac{1}{\gamma(V)}\int \alpha_m(V)d\gamma(V) \tag{13}$$

The equation (12) and (13) are the basic equations in the model of EAM modulator and extensive simulations can be performed by evaluating the performance of EAM modulator with respect to the variation in applied bias or modulation voltage for specific set of absorption and alpha-parameters of the absorption layer of EAM modulator.

Further, the chirp in the externally modulated signals is significantly low but still this needs to be controlled. The frequency chirp is defined by the variation in the phase of the signal with respect to the time which is given by equation (14) [30, 31].

$$\Delta\nu(t) = \frac{1}{2\pi}\frac{d\phi}{dy} = \frac{\alpha(V,N)}{4\pi}\frac{d\ln(P_{out}(V,N))}{dt} \tag{14}$$

Here in equation (14), ϕ is the phase of modulated optical signal, α is the α-parameter and P_{out} is the output signal power. These α-parameter depend on the applied signal voltage. So, in order to reduce the chirp factor in the output of EAM modulator, the reverse bias voltage play an important role and -2.5 is the desirable reverse bias voltage in terms of high conversion efficiency and negative chirp factor [32].

Variation in alpha parameter and absorption of EAM modulator with respect to the applied signal voltage at wavelength 1557.16 [30, 31] is shown in Fig. 4. From equation (10) and (11), it can be clearly seen that, for a particular frequency signal, the transparency of the EAM modulator strictly dependent on the reverse-biased voltage applied to the EAM modulator [20, 30-31]. When the reverse-biased voltage level is high, a large number of photon assisted carrier absorption generated charged carriers induces drift and diffusion of these carriers distorted and screen the external electric field and saturate the absorption coefficient [22, 23].

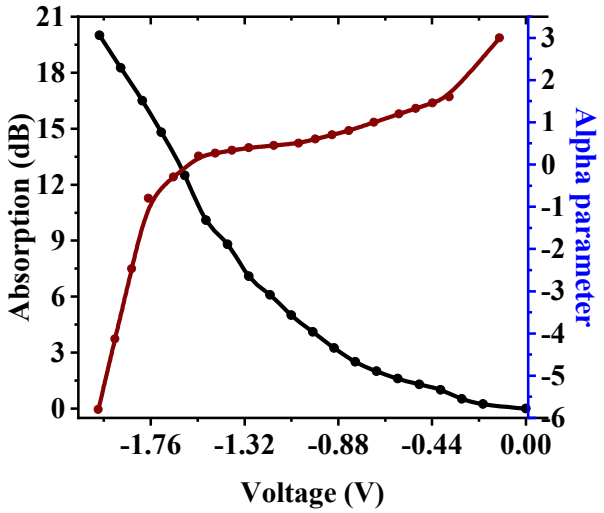

Fig. 4. Converted signal quality signal under fixed reverse bias voltage (colour online)

Here the reverse biased voltage and modulation voltage (peak to peak) applied to the EAM modulator are -2.5 V and 2 V respectively. EAM modulator behaves like a transparent device to the optical signal in the absence of an electrical signal and an opaque device to the optical signal in the presence of an electrical signal. Further, the sinusoidal electrical signal is applied to the EAM simply behave as double-sideband modulation scheme (DSB-SC modulation) which shifts the spectrum of the input optical

signals to the upper sideband (USB) and lower sideband (LSB) with multiple harmonics having frequency difference equal to the frequency of the sinusoidal electrical signal, which is clearly shown in Fig. 5 and the input and output frequencies of USB and LSB are described in Table 1.

Table 1. Wavelength-converted signals with applied input

Input Signal →		*192.8 THz*	*193.34 THz*
Wavelength-converted signal (THz) ↓	*USB*	*193.175 THz*	*193.715 THz*
		193.550 THz	*194.09 THz*
	LSB	*192.425 THz*	*192.965 THz*
		192.05 THz	*192.590 THz*

In Fig. 5(b), it is observed that higher the harmonics of wavelength-converted signal, lower will be the amplitude of wavelength-converted signal. So, to minimize the effect of adjacent wavelength-converted signals, USB of wavelength shifted signal f2 and LSB of wavelength shifted signal f1 is considered. As a result, the signal at frequency 193.715 THz and 192.425 THz are the best values of wavelength shifted signals in terms of low power penalty. Furthermore, the optical signals having different wavelength propagate through EAM based wavelength converter, the crosstalk between wavelength-converted signal can be avoided by the proper adjustment of the frequency of the electrical signal which is provided to EAM. The frequency of the electrical signal and maximum bandwidth of message signal for particular electrical signal frequency and fixed channel spacing can be calculated by equation (2), (3), (5) and (6).

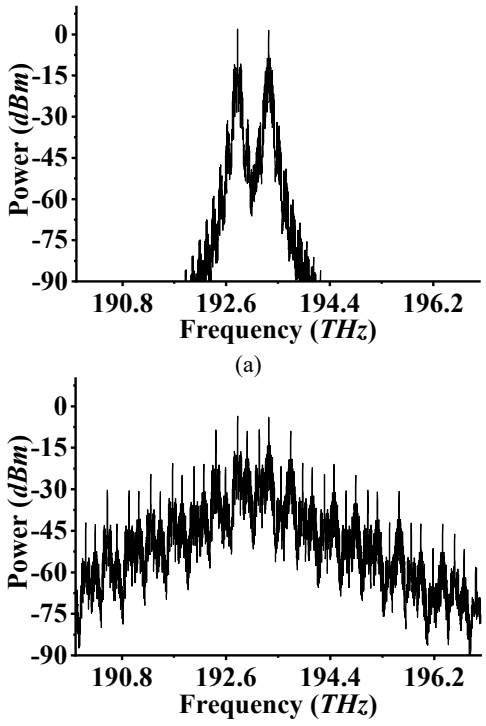

Fig. 5. Spectrum diagrams of signals (a) before and (b) after co-propagating through EAM

Further, the signal from the EAM modulator is followed by de-multiplexer. These wavelengths converted signals are separate out by the use of de-multiplexer. Other signals specified in Table 1 can be used as wavelength-converted signals and can be separated by the use of de-multiplexer. These wavelengths shifted signals are further analysed by the receiver section. The timing diagram of output signals received at frequency 193.715 THz and 192.425 THz are shown in Fig. 2 (c) and (d) respectively. From the timing diagram, it has been observed that the amplitude of the wavelength-converted signal gets distorted due to various nonlinearities and carrier lifetime inside the active medium of EAM. This amplitude irregularity can be determined for the digital communication system [24]. Furthermore, these irregularities in the amplitude can be reduced by propagating the signal through a SOA with optically modified gain dynamics in conjunction with a Micro-ring Resonator (MRR) based notch filter [25].

3. Results and discussion

To evaluate the performance of the designed multi-channel wavelength converter, all the simulations are carried out at the data rate of 120 Gbps in Optisystem-16.0. Fig. 6 shows the power level of uplink and downlink multi-channel wavelength-converted signals given in Table 1 and it is analysed that power level decreases with the increase in the order of harmonics of wavelength converted signal.

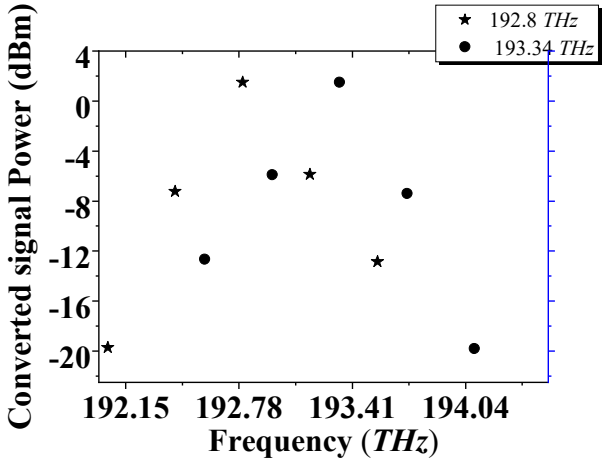

Fig. 6. Plot between signal power level versus converted signal frequency

So to decrease the effect of cross talk and increase the quality (Q-factor) of multi-channel wavelength-converted signals the signal at 193.715 (replica of the signal at frequency 193.34 THz) and 192.425 THz (replica of 192.8 THz) are considered.

After the selection of the frequency for the best replica of wavelength-converted signals, the effect of the input signal power on the wavelength-converted signal power is analysed and it is observed that with the increase

in the input signal power, the output signal power increases linearly. The plot between input signal power (P_1, P_2) versus output signal power P_{11} (192.425 THz) and P_{21} (193.715 THz) is shown in Fig. 5.

Further, the system is analysed in terms of quality factor (Q-factor). The Q-factor is given by equation (15) [26].

$$Q = \frac{\bar{P}_1 - \bar{P}_0}{\sigma_1 + \sigma_0} \tag{15}$$

Here in equation (1) $\bar{P}_1, \bar{P}_0$ and σ_1, σ_0 are the mean and standard deviation of peak power of the level high and level low. The Q-factor value should be above 15 dB for a successful reception at the receiver end [26]. Fig. 8 shows the variation in the quality factor of wavelength-converted signals for the input signal power. In Fig. 8, P_1 and P_2 are the input signal powers at the wavelength of 192.8 THz and 193.34 THz respectively. Simultaneously, results at different power levels show that with the increase in input signal power P_1 at constant input signal power P_2, the quality (Q_1) of wavelength-converted signal at frequency 192.425 THz increases and the quality (Q_2) of the frequency-converted signal at wavelength 193.715 decreases and vice versa.

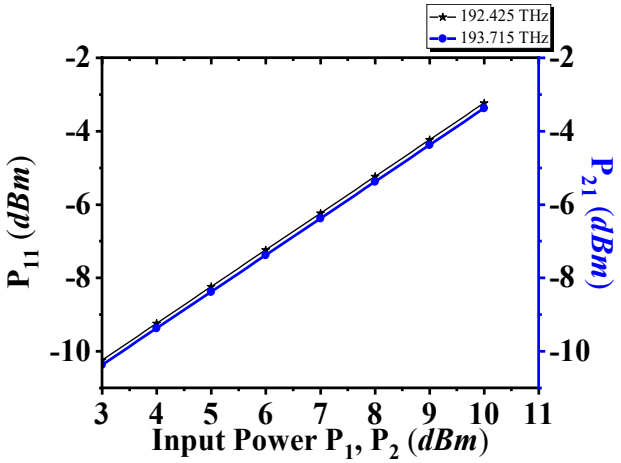

Fig. 7. Input signal power versus wavelength-converted signal power (colour online)

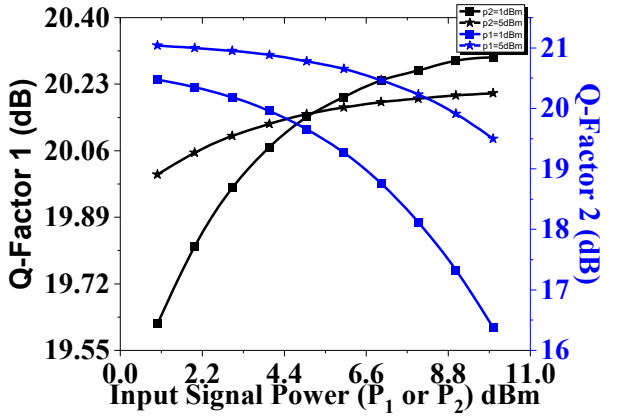

Fig. 8. Plot between input signal powers versus output signal quality factor (colour online)

This is due to an increase in P_1, the EAM becomes more and more transparent which decreases the effect of the electrical signal on the signal at P_2, which ultimately decreases the quality Q_2 at constant power P_2. Similarly, with the increase in input signal power P_2 at constant P_1, the Q_2 increases, and Q_1 decreases.

The channel spacing between two copropagating signals also plays an important role in the design of a multi-channel wavelength converter. The effect of channel spacing on the quality of the output signal at the data rate of 120 Gbps is analysed and the plot between the quality factor of converter signals versus channel spacing is drawn in Fig. 9. The value for electrical signal frequency is calculated from equation (2). From the plot, it can be seen that initially when the channel spacing is very low, due to cross-talk between input data signals no wavelength conversion will be there. With the increase in channel spacing, input data signal cross talk decreases, but LSB and USB of wavelength-converted signal interfere with adjacent data signals which result in the poor quality of wavelength-converted signal. With a further increase in channel spacing, the cross-talk decreases linearly. As the channel spacing reaches the limit specified in equation (1), significant wavelength conversion operation comes into the picture. The good quality factor is observed with increase in channel spacing. With further increase in the channel spacing, the quality of wavelength-converted signal reaches the saturation.

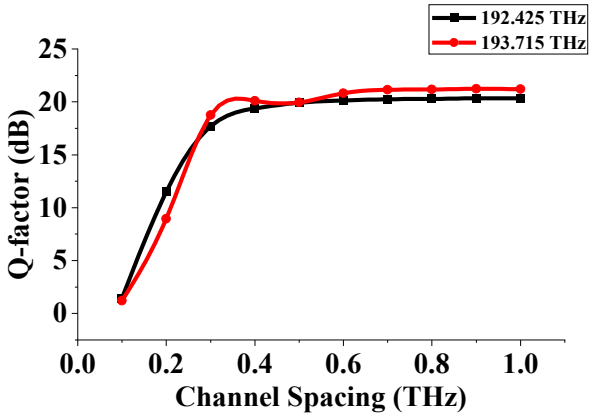

Fig. 9. Plot between channel spacing versus output signal quality factor (colour online)

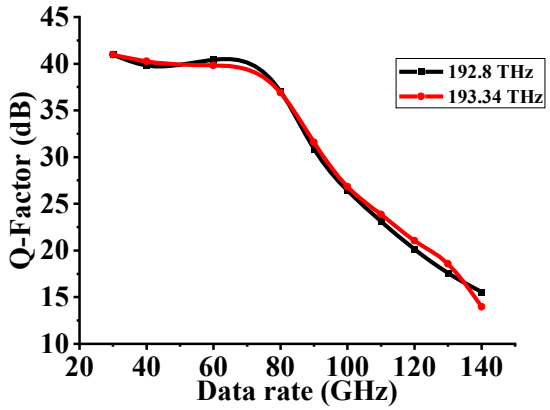

Fig. 10. Plot between input signal data rate versus output signal quality factor (colour online)

The optimum channel spacing observes from the channel spacing analysis for the design of a multi-channel wavelength converter operating at the data rate of 120 Gbps is 540 GHz.

Now, the effect of data rate on the quality of wavelength-converted signal is observed at a constant channel spacing of 540 GHz and electrical signal frequency as of 375 GHz. The plot between output signal Q-factor versus input data rate is shown in Fig. 10. From the plot, it is observed that with the increase in input signal data rate, wavelength-converted signal quality decreases. Initially, when the data rate is very low, the wavelength converter reveals excellent quality factor. With the significant increase in input signal data rate, the output wavelength signal quality factor also decreases significantly. Once the data rate becomes more than 120 GHz, the wavelength-converted signal quality goes down to 15 dB.

Further, the optimization in the input signal power, channel spacing, and maximum signal data rate, the eye diagram of the wavelength-converted signal at the frequency of 192.425 THz, and 193.715 THz are shown in Fig. 11. Eye-opening distinguishes the envelopes for level high and level low [27]. This should be as high as much as possible. Somewhere this gives the idea of signal Q-factor. From Fig. 11, it has been concluded that the level high and level low are easily distinguishable which results in the error-free output. The higher the value of eye-opening better will be the signal quality. The Q-factor of the wavelength-converted signal at frequency 192.425 THz and 193.715 THz is 20.25 dB and 21.14 dB respectively for the applied signal at 192.8 THz and 193.34 THz.

4. 4-channel wavelength converter

The proposed design for the 4-channel wavelength conversion simultaneously is shown in Fig. 12. The design consists of four transmitters in the input blocks at the data rate of 10 Gbps having a centre frequency of 192.8 THz, 192.9 THz, 193 THz, and 193.1 THz. Signals from four transmitters followed by multiplexer, which is further followed by an EAM modulator derived by 75 GHz electrical signal generator. The 75 GHz value is chosen by applying the same interference-avoidance framework derived earlier (Equations (2), (3), (5), and (6) of the manuscript) to the 10 Gbps, closely spaced 4-channel case. The driving frequency satisfies the conditions on maximum message bandwidth and channel spacing such that (i) the generated upper and lower sidebands of each channel do not overlap with neighbouring data channels and (ii) adequate spectral separation is maintained between desired converted tones and adjacent harmonics to minimize inter-channel crosstalk. Multiple wavelength-converted signals have been received at the demultiplexer end and analysed at the receiver section. The optical spectrum at the multiplexer end and EAM output port is shown in Fig. 12 (a) and (b). The quality factor of 30 dB, 29.5 dB, 22 dB, and 30.2 dB of the signal received at 192.725 THz, 192.825 THz, 193.075 THz, and 193.175 THz respectively corresponding to the input signal of 192.8 THz,192.9 THz, 193 THz, and 193.1 THz.

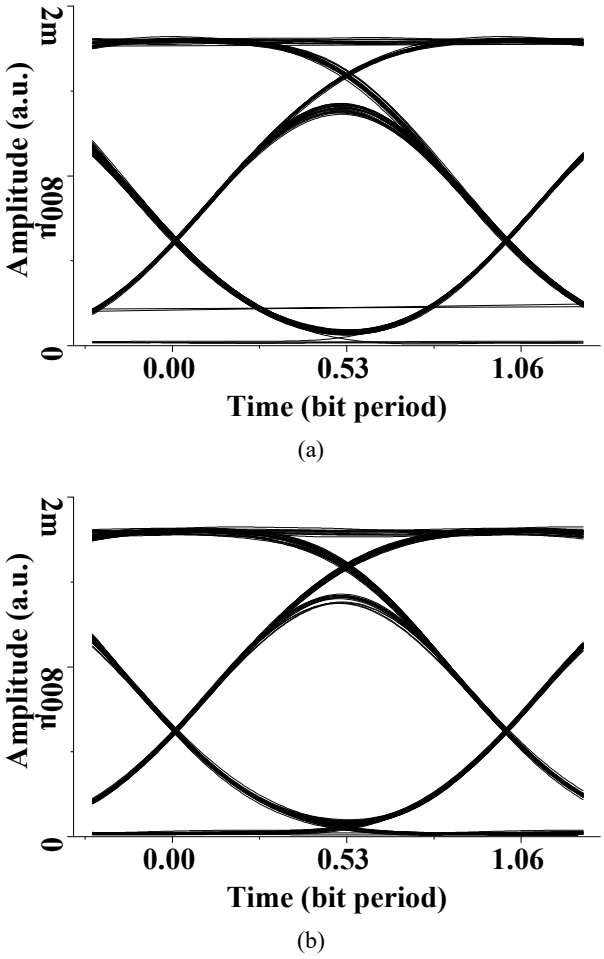

Fig. 11. Eye diagrams of wavelength-converted signal at (a) 192.42 THz and (b) 192.715 THz

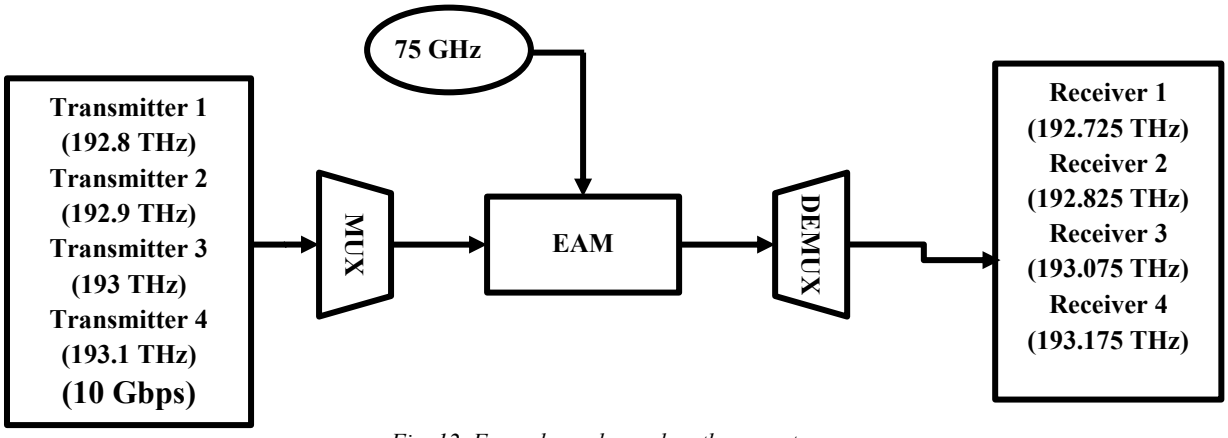

Fig. 12. Four-channel wavelength converter

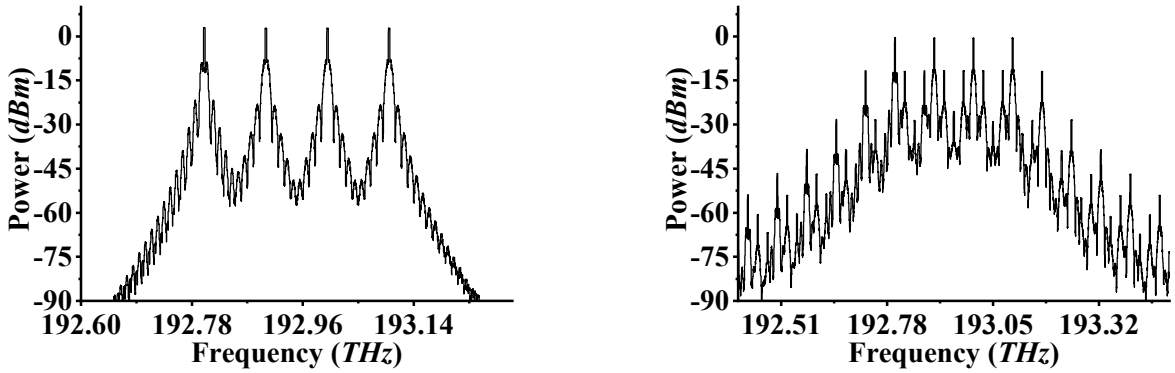

(a) (b)

Fig. 13. Optical spectrums of (a) 4-channel input signal and (b) wavelength converted output signal

Table 2. Comparison of the proposed work with current state of the art

Parameter	Proposed Work	Kaur et al. [33]	Singh et al. [34]	Zhou et al. [35]	Zhao et al. [36]
Wavelength conversion technique	XAM in EAM	XAM in EAM	FWM in HNLF	FWM in SOA	FWM in dual-polarization SOA
Operating speed	120 Gbps	40 Gbps	100 Gbps	30 Gbps	112 Gbps
Polarization sensitivity	Insensitive	Insensitive	Sensitive	Sensitive	Sensitive
Integration possibility	Possible	Possible	Not Possible	Possible	Possible
Modulation Format	NRZ	NRZ	DP-DQPSK	16QAM-OFDM	PDM-16QAM

In order to position the proposed EAM-based multi-channel wavelength converter with respect to existing solutions, a concise state-of-the-art comparison of the present work with recently reported wavelength conversion schemes is presented in Table 2.

5. Conclusions

The investigation demonstrates a multi-channel wavelength conversion approach for widely spaced channels using cross-absorption modulation (XAM) in an EAM modulator. System performance strongly depends on input signal power, channel spacing, and input data rate. Output signal quality improves with increased channel spacing and decreases with higher input data rates. Additionally, output signal power increases linearly with input power. The proposed system is further extended to a 4-channel wavelength conversion design, showcasing high conversion efficiency and quality factors exceeding 20 dB for each channel. This system represents a scalable, efficient solution for high-speed optical networks, emphasizing its potential for future multi-channel applications.

Acknowledgement

Authors would like to thank SERB, New Delhi for the funding of CRG project vide sanction order no: CRG/2022/001866 dated: 30-01-2023.

References

[1] D. Singh, S. Singh, V. Sharma, S. Singh, Q. M. Ngo, Optical and Quantum Electronics **51**, 215 (2019).
[2] S. Singh, D. Singh, V. Sharma, S. Singh, Q. M. Ngo, Optical Fiber Technology **52**, 101958 (2019).
[3] S. Singh, Opt. Commun. **281**(9), 2618 (2008).
[4] H. Zhou, J. He, Z. Dong, Y. Cheng, L. Chen, Opt. Commun. **316**, 161 (2014).
[5] J. Gao, M. A. Vincenti, J. Frantz, A. Clabeau, X. Qiao, L. Feng, M. Scalora, N. M. Litchinitser, Nanophotonics **11**(17), 4027 (2022).
[6] Y. Liu, E. Tangdiongga, Z. Li, Huug de Waardt, A. M. J. Koonen, G. D. Khoe, Xuewen Shu, Ian Bennion, H. J. S. Dorren, J. Lightwave Technol. **25**(1), 103 (2007).
[7] P. Zhao, Zonglong He, Vijay Shekhawat, Magnus Karlsson, Peter A. Andrekson, Nanophotonics **12**(17), 3427 (2023).
[8] J. Wei, C. Chen, Y. Wu, C. Zeng, M. Tang, J. Xia, J. Lightwave Technol. **42**(17), 5966 (2024).
[9] D. Krcmarik, M. Karasek, J. Radil, J. Vojtech, Opt. Commun. **278**(2), 402 (2007).
[10] S. Singh, R. S. Kaler, Opt. Commun. **118**, 390 (2007).
[11] M. R. Fernández-Ruiz, Lei Lei, M. Rochette, J. Azana, Opt. Express **23**, 22847 (2015).
[12] P. Honzatko, Opt. Commun. **283**(9), 1744 (2010).
[13] W. Hong, M. Li, X. Zhang, J. Sun, D. Huang, J. Lightwave Technol. **27**(24), 5580 (2009).
[14] K. Obermann, S. Kindt, D. Breuer, K. Petermann, J. Lightwave Technol. **16**(1), 78 (1998).
[15] E. D. Ellis, A. E. Kelly, D. Nesset, D. Pitcher, D. G. Moodie, R. Kashyap, Electron. Lett. **34**(20), 1958 (2002).
[16] W. Li, Wen Hui Sun, Wen Ting Wang, Ning Hua Zhu, Opt. Lett. **39**(9), 2672 (2014).
[17] S. H. Lee, H. J. Kim, J. I. Song, IEEE Photonic. Tech. L. **25**(18), 1812 (2013).
[18] J.-H. Seo, Chang-Soon Choi,Young-Shik Kang, Yong-Duck Chung, Jeha Kim, Woo-Young Choi, 2005 International Topical Meeting on Microwave Photonics (2005).
[19] N. El Dahdah, R. Coquille, B. Charbonnier, E. Pincemin, C. Kazmierski, G. Aubin, 2005 Pacific Rim Conference on Lasers & Electro-Optics, CLEO - Tech. Dig. 2005, 538 (2005).
[20] J. P. R. Lacey, S. J. Madden, M. A. Summerfield, IEEE Photonic. Tech. L. **9**(10), 1355 (1997).
[21] K. K. Chow, C. Shu, Opt. Express **12**(13), 3050 (2004).
[22] Y. Yang, C. Lou, J. Wang, L. Huo, Y. Gao, Opt. Commun. **260**, 571 (2006).
[23] T. H. Wood, John Z. Pastalan, Charles A. Burrus, Jr. Bart C. Johnson, Barry I. Miller, Jose L. deMiguel, Uziel Koren, Martin G. Young, Appl. Phys. Lett. **57**, 1081(1990).
[24] J. S. Vardakas, K. E. Zoiros, Opt. Eng. **46**(8), art. 085005, 1 (2007).
[25] Z. V. Rizou, K. E. Zoiros, A. Hatziefremidis, Opt. Commun. **329**, 206 (2014).
[26] E. Dimitriadou, K. E. Zoiros, Progress Electromagnetics Research B (PIERS) **50**, 113 (2013).
[27] D. K. Gayen, T. Chattopadhyay, K. E. Zoiros, J. Comput. Electron. **14**, 129 (2015).
[28] G. B. Morrison, James W. Raring, Chad S. Wang, Erik J. Skogen, Yu-Chia Chang, Matt Sysak, L. A. Coldren, Solid State Electron. **51**, 38 (2007).
[29] D. S. Chemla, Phys. Today **38**(5), 56 (1985).
[30] J. C. Cartledge, B. Christensen, J. Lightwave Technol. **16**(3), 349 (1998).
[31] N. Cheng, J. C. Cartledge, J. Lightwave Technol. **23**(12), 4265 (2005).
[32] M. Y. Jamro, J. M. Senior, Photonic Netw. Commun. **10**(2), 267 (2005).
[33] T. Kaur, S. Singh, Lovkesh, E. A. Anashkina, A. V. Andrianov, Optoelectron. Adv. Mat. **15**(7–8), 307 (2021).
[34] S. Singh, S. Singh, Q. M. Ngo, A. M. Mohammadi, Opt. Fiber Technol. **59**, 102323 (2020).
[35] H. Zhou, Y. Shen, M. Chen, C. Fei, J. He, Opt. Express **27**, 38553 (2019).
[36] Y. Zhao, Z. Yan, P. Fu, Y. Cai, Y. Yuan, OSA Continuum **4**, 1125 (2021).

*Corresponding author: surinder_sodhi@rediffmail.com